AD-A162 852 CRACK GROWTH BEHAVIOR OF ALUMINUM ALLOYS TESTED IN LIQUID MERCURY(U) ARMY ARMAMENT RESEARCH AND DEVELOPMENT CENTER WATERVLIET NY L.. J A KAPP ET AL. 1/1

UNCLASSIFIED SEP 85 ARLCB-TR-85034 SBI-AD-E440 309 F/G 11/6 NL

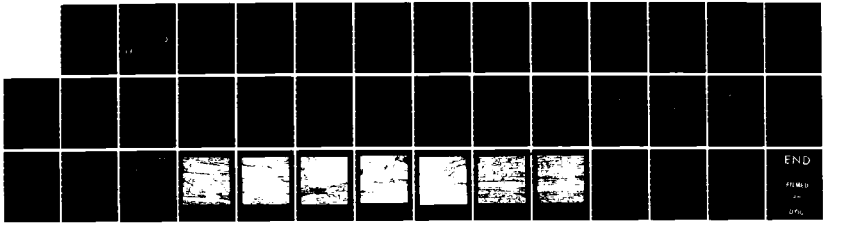

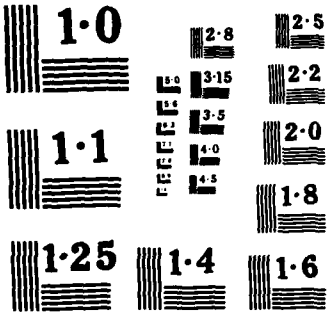

NATIONAL BUREAU OF STANDARDS
MICROCOPY RESOLUTION TEST CHART

(12)

AD-A162 852

AD E440 309

TECHNICAL REPORT ARLCB-TR-85034

CRACK GROWTH BEHAVIOR OF ALUMINUM ALLOYS TESTED IN LIQUID MERCURY

J. A. KAPP

D. J. DUQUETTE

M. H. KAMDAR

SEPTEMBER 1985

US ARMY ARMAMENT RESEARCH AND DEVELOPMENT CENTER
LARGE CALIBER WEAPON SYSTEMS LABORATORY
BENÉT WEAPONS LABORATORY
WATERVLIET N.Y. 12189

DISCLAIMER

The findings in this report are not to be construed as an official Department of the Army position unless so designated by other authorized documents.

The use of trade name(s) and/or manufacture(s) does not constitute an official indorsement or approval.

DISPOSITION

Destroy this report when it is no longer needed. Do not return it to the originator.

SECURITY CLASSIFICATION OF THIS PAGE (When Data Entered)

REPORT DOCUMENTATION PAGE		READ INSTRUCTIONS BEFORE COMPLETING FORM
1. REPORT NUMBER ARLCB-TR-85034	2. GOVT ACCESSION NO. AD-A162 852	3. RECIPIENT'S CATALOG NUMBER
4. TITLE (and Subtitle) CRACK GROWTH BEHAVIOR OF ALUMINUM ALLOYS TESTED IN LIQUID MERCURY		5. TYPE OF REPORT & PERIOD COVERED Final 6. PERFORMING ORG. REPORT NUMBER
7. AUTHOR(s) J. A. Kapp, D. J. Duquette (see reverse), and M. H. Kamdar		8. CONTRACT OR GRANT NUMBER(s)
9. PERFORMING ORGANIZATION NAME AND ADDRESS US Army Armament Research & Development Center Benet Weapons Laboratory, SMCAR-LCB-TL Watervliet, NY 12189-5000		10. PROGRAM ELEMENT, PROJECT, TASK AREA & WORK UNIT NUMBERS AMCMS No. 6111.02.H600.011 PRON No. 1A425M541A1A
11. CONTROLLING OFFICE NAME AND ADDRESS US Army Armament Research & Development Center Large Caliber Weapon Systems Laboratory Dover, NJ 07801-5001		12. REPORT DATE September 1985 13. NUMBER OF PAGES 32
14. MONITORING AGENCY NAME & ADDRESS(if different from Controlling Office)		15. SECURITY CLASS. (of this report) UNCLASSIFIED 15a. DECLASSIFICATION/DOWNGRADING SCHEDULE

16. DISTRIBUTION STATEMENT (of this Report)

Approved for public release; distribution unlimited.

17. DISTRIBUTION STATEMENT (of the abstract entered in Block 20, if different from Report)

18. SUPPLEMENTARY NOTES

Presented at ASME Symposium on Crack Growth Behavior of Material Susceptible to Stress Corrosion, New Orleans, LA, December 1984.
Submitted to ASME Journal of Engineering Materials and Technology.

19. KEY WORDS (Continue on reverse side if necessary and identify by block number)

Fracture Mechanics
Liquid Metal Embrittlement
Aluminum Alloys
Mechanisms
Fracture

20. ABSTRACT (Continue on reverse side if necessary and identify by block number)

Crack growth rate measurements have been made in three mercury embrittled aluminum alloys each under three loading conditions. The alloys were 1100-0, 6061-T651, and 7075-T651. The loading conditions were fixed displacement static loading, fixed load static loading, and fatigue loading at two frequencies. The results showed that mercury cracking of aluminum was not unlike other types of embrittlement (i.e. hydrogen cracking of steels). Under
(CONT'D ON REVERSE)

7. AUTHORS (CONT'D)

D. J. Duquette
Materials Engineering Department
Rensselaer Polytechnic Institute
Troy, NY 12181

20. ABSTRACT (CONT'D)

fixed load static conditions no crack growth was observed below a threshold stress intensity factor (K_{ILME}). At K levels greater than K_{ILME} cracks grew on the order of cm/s, while under fixed displacement loading, the crack growth rate was strongly dependent upon the strength of the alloy tested. This was attributed to crack closure. In the fatigue tests, no enhanced crack growth occurred until a critical range of stress intensity factor (ΔK_{th}) was achieved. The ΔK_{th} agreed well with the K_{ILME} obtained from the static tests, but the magnitude of the fatigue growth rate was substantially less than was expected based on the static loading results. Observations of the fracture surfaces in the scanning electron microscope (SEM) suggested a brittle intergranular fracture mode for the 6061-T651 and the 7075-T651 alloys under all loading conditions. The fractographic features of the 1100-0 alloy under fixed load and fatigue loading conditions were also brittle intergranular. Under fixed displacement loading the cracks grew via a ductile intergranular mode.

TABLE OF CONTENTS

TABLES

LIST OF ILLUSTRATIONS

INTRODUCTION

Fracture mechanics test methods have been helpful in the study of environmentally assisted fracture phenomena (refs 1-3). Although powerful, these methods have been used only sparingly in the study of liquid metal embrittlement (LME). The purpose of this study was to thoroughly examine the crack growth behavior of an LME couple: aluminum-mercury. Several variables were studied. Three aluminum alloys were tested to study the effects of yield strength on crack growth. The loading conditions were changed such that each alloy was studied under fixed displacement loading, fixed load loading, and fatigue loading. Furthermore, two fatigue loading frequencies were tested.

MATERIALS

The three aluminum alloys studied were commercially pure aluminum (1100) in the annealed conditions; the Mg-Si-Al alloy 6061 in the T651 condition (solution treated, stress relieved by stretching and aged); and the Zn-Mg-Cu-Al alloy, 7075 also in the T651 condition. Rolled sheets of these alloys were obtained. Specimens were machined such that the long transverse properties were measured. Table I shows the mechanical properties of each of these alloys.

---

[1]Wei, R. P., Novak, S. R., and Willians, D. P., Matls. Res. Stand., Vol. 12, 1972, p. 25.
[2]Wei, R. P. and Landes, J. D., Matls. Res. Stand., Vol. 9, No. 7, 1969, p. 9.
[3]Clark, W., J. of Materials for Energy Systems, Vol. 1, 1980, p. 35.

TABLE I. MECHANICAL PROPERTIES OF THE ALLOYS TESTED

Alloy	.1% σ_{ys} MPa	σ_{ys} MPa	% RA	% Elongation	K_{Ic} (MPa$\sqrt{m}$)
1100-0	27.7	71.6	90.6	52.8	45.5
6061-T651	282.0	312.3	35.7	14.3	31.5
7075-T651	517.1	590.3	18.2	12.8	30.5

SPECIMEN DESIGN

The specimen used to measure crack growth rates is pictured in Figure 1, a modified compact tension with side grooves. Load (P) was transmitted through the pin holes and the crack mouth opening displacement (CMOD) was measured as indicated. The side grooves were included to reduce unstable crack branching.

The stress intensity factor (K) solution was given by Gross and Srawley (ref 4). The CMOD solution was developed by Kapp (ref 5) using finite elements. Using the methods outlined in Reference 6, the numerical K solution was approximated as a continuous function of relative crack length, (a/W) by:

$$\frac{KB\sqrt{W}(1-a/W)^{3/2}}{P\,(1.7 + a/W)} = f(a/W) \qquad (1)$$

---

[4]Gross, B. and Srawley, J. E., "Stress Intensity Factors For Boundary Collocations for Single-Edge Notch Specimens Subject to Splitting Forces," NASA TN D-3295, 1966.

[5]Kapp, J. A., "Crack Growth in Mercury Embrittled Aluminum Alloys Under Cyclic and Static Loading Conditions," Ph.D. Thesis, Rensselaer Polytechnic Institute, Troy, NY, May 1982.

[6]Kapp, J. A., Newman, J. C. Jr., and Underwood, J. H., Journal of Testing and Evaluation, JTEVA, Vol. 8, No. 6, November 1980.

$$f(a/W) = 1.84 + 2.81(a/W) - 12.9(a/W)^2 + 16.1(a/W)^3 - 6.41(a/W)^4 \quad (2)$$

where B is the geometric mean of B_1 and B_2 ($B = \sqrt{B_1 B_2}$), and the other variables are defined in Figure 1. Equations (1) and (2) agree with the numerical K solution to within 0.5 percent over the change $0.2 \leq a/W \leq 1.0$.

The CMOD solution was developed such that we had a method to remotely measure the relative crack length. An expression similar to Eqs. (1) and (2) was developed to represent the finite element CMOD solution. First we developed the dimensionless parameter δ'

$$\delta' = \ell n \left(\frac{EB(CMOD)}{P}\right) \quad (3)$$

where E is Young's modulus.

The relative crack depth was then found to be:

$$a/W = 0.1351 - 0.1874\delta' + 0.1117(\delta')^2 - 0.012(\delta')^3 \quad (4)$$

This equation is valid over the range $0.0833 \leq a/W \leq 0.833$ to within ± 3.5 percent of the numerical solution.

EXPERIMENTAL PROCEDURE

Three types of loading were studied. In the fatigue loading tests, specimens were tension-tension cycled at two frequencies (30 Hz and 5 Hz) at a constant R ratio ($R = K_{min}/K_{max} = 0.1$). During the testing, the CMOD range was constantly measured. Since the load range (ΔP) was held constant, we had sufficient information to use Eqs. (3) and (4) to determine the crack length as a function of loading cycles (N). Once the crack length and N were known, a plot was generated and the fatigue crack growth rate (da/dN) was determined at several values of a. This was accomplished by graphical differentiation. The stress intensity factor range (ΔK) was also calculated using Eqs. (1) and

(2), and the results were then plotted in the usual manner.

The two static loading conditions were fixed displacement and fixed load. For either test the specimen was first fatigue precracked to produce an embrittled crack. A fixed displacement test was conducted by the rapid application of a large CMOD to the specimen. After the initial loading the large CMOD was maintained until the completion of the test. This resulted in crack propagation at a high K initially followed by a shedding of the load such that the crack arrested. The fixed load tests were conducted by slowly increasing the applied load until crack propagation occurred. While the crack advanced, the load was held constant until the specimen fractured.

Under the static test conditions, it was necessary to simultaneously measure both the load and CMOD to use Eqs. (3) and (4) to determine the crack length. This was accomplished on a dual channel strip chart recorder. Using these measurements, the crack length was then known as a function of time. Using the method described above, the crack velocity (da/dt) and applied K were determined and plotted on semilog graph paper.

WETTING PROCEDURE

One of the prerequisites for LME is good wetting of the solid metal with the liquid species. Aluminum is very difficult to wet with mercury. To overcome this problem, a unique method was developed. The aluminum specimens were plated with a thin (about 0.025 mm) coating of copper. The copper was then coated with a saturated aqueous solution of mercurous nitride. A thin layer of mercury was deposited on the copper by chemical displacement. The aqueous solution was then removed and additional liquid mercury was added

to the areas covered by the chemically displaced coating. This resulted in excellent wetting. Embrittlement occurred once the copper coating was broken via fatigue loading of the sample. Since we were only interested in crack propagation in the aluminum, this wetting method was totally adequate.

FATIGUE CRACK GROWTH RESULTS

The results of the fatigue crack growth tests are shown in Figures 2 through 4 for the 1100, 6061, and 7075 alloys respectively. In all these plots the open symbols represent crack growth rate measurements obtained from testing in laboratory air, and the solid symbols represent data from testing performed in mercury. As was expected, the results of the tests in air followed the Paris power law. Also, severe embrittlement was observed in all of the alloys in mercury.

These results, treated as an aggregate, showed that the fatigue crack growth phenomenon of mercury embrittled aluminum is not unlike hydrogen embrittled steel (ref 7). Specifically, below a certain ΔK_{th} there was no effect of the mercury on crack growth. Once ΔK_{th} was exceeded, the fatigue crack growth rate increased very quickly with increasing ΔK. This initial region was followed by a range of ΔK where the crack growth rate increased very little.

In the results from the testing of 6061 and 7075 there was an effect of loading frequency on crack growth rate. At the low frequency (5 Hz), the crack growth rate was as much as two orders of magnitude greater than at the

---

[7]Wei, R. P., in Fatigue Mechanisms, Fong, J. T., Ed., ASTM STP 675, ASTM, Philadelphia, PA, 1979, p. 816.

higher frequency (30 Hz) in 7075. In 6061, the maximum difference was no greater than about a factor of 50. Although the distinct frequency effect was not observed in 1100, the maximum crack growth rate measured at 5 Hz was about an order of magnitude greater than the maximum rate observed at 30 Hz. The effect of frequency was not unlike the frequency effect observed in other environmentally assisted fracture phenomena (ref 7).

STATIC LOADING CRACK VELOCITY RESULTS

The crack velocity measurements obtained under both fixed load and fixed displacement conditions are shown in Figures 5, 6, and 7 for 1100, 6061, and 7075 respectively. Considering the load control tests first, we observed the following. In all materials no crack growth was observed below a threshold K level (K_{ILME}). Once the applied K was greater than K_{ILME}, the crack velocity increased almost as a step function to a rate of between 4 cm/s and 10 cm/s, where it remained constant until the specimens fractured. The crack velocity decreased to about 1 cm/s or 2 cm/s in 1100 before fracture occurred. Again, this behavior was similar to that observed in hydrogen embrittled steel (ref 3).

The results obtained in the fixed displacement testing showed a much different behavior. In these tests the specimens were loaded very rapidly to a high K level. For 1100 and 6061, the initial loading was not sufficiently fast to prevent crack growth upon rising load. Thus, we observed crack growth

---

[3]Clark, W., J. of Materials for Energy Systems, Vol. 1, 1980, p. 35.
[7]Wei, R. P., in Fatigue Mechanisms, Fong, J. T., Ed., ASTM STP 675, ASTM, Philadelphia, PA, 1979, p. 816.

behavior similar to that observed under the fixed load conditions. This was to be expected since as the crack grew, the application of the external load resulted in an increase in K. Once the maximum K was attained further crack growth resulted in a reduction of the external load which caused K to decrease. Under these conditions, the behavior was different for each alloy. In the 1100 alloy, the crack arrested at a very high K level. The 6061 alloy exhibited crack growth behavior wherein the crack velocity decreased by about an order of magnitude and remained constant. When K was reduced to a sufficiently low level, the crack arrested. K_{ILME} under these conditions was somewhat lower than that necessary to initiate accelerated growth in the fixed load tests. Finally, in the case of 7075, the crack grew at the same velocity regardless of the loading condition. Also, K_{ILME} was smaller in displacement control for 7075.

SEM OBSERVATIONS OF THE FRACTURE SURFACES

The fracture surface created in the embrittled fatigue test of 1100 is shown in Figure 8. The appearance suggested an intergranular fracture mode as evidenced by the clear outline of the grain in the center of the figure (position A), and in the many secondary cracks at other grain boundaries. There was also some evidence of a more ductile fatigue fracture appearance (position B).

Figures 9 and 10 show the fracture surfaces created in the fixed load testing of 1100. The features of this surface were substantially different than those observed in the fatigue tests. The fracture mode was predominantly intergranular, but there were a great deal of dimples. Also, there was more secondary cracking. At higher magnification (Figure 10), the dimples were centered around secondary, insoluble particles. The density of dimples was greater in the secondary cracks, where the fracture appeared to be very ductile.

Under the fixed displacement loading conditions (Figure 11), the fracture appearance was similar to that observed in the fatigue testing of 1100. The fracture mode was predominantly brittle intergranular with some secondary cracking of the grain boundaries. There was also some evidence of brittle transgranular cracking as observed by the cleaved grain in the center of the figure. Additionally, there were some of the small dimples similar to those observed in the fixed load case.

The surfaces created during the testing of 6061 are shown in Figures 12 and 13. The embrittled fatigue surface (Figure 12) indicated a brittle intergranular fracture mode with very little secondary cracking. Under either fixed load or fixed displacement loading conditions, the same fracture surface resulted (Figure 13). The fracture mode was intergranular essentially without secondary cracking. The fracture event was apparently accompanied by the formation of large but shallow dimples on the grain boundaries.

Mercury embrittled crack growth in 7075 resulted in the same fracture appearance regardless of loading condition. Under fatigue loading (Figure 14), the fracture mode was brittle intergranular with some secondary cracking.

The outlines of the long elongated grains were clearly visible. Figure 15 demonstrates that under either of the static loading conditions, the same brittle intergranular fracture surface appearance was created.

DISCUSSION

Static Loading Results

Testing under fixed load or fixed displacement gave two measures of the degree of embrittlement: K_{ILME} and the magnitude of steady state crack velocity $(da/dt)_{ss}$. The results obtained are summarized in Table II. The K_{ILME} data reported in the table were the lowest measured threshold K values (i.e. fixed displacement for 6061 and 7075; fixed load for 1100). Presentation of the data in this manner enabled us to discuss some interesting correlations between embrittlement and yield strength.

TABLE II. SUMMARY OF STATIC LOADING RESULTS

Alloy	.1% σ_{ys} (MPa)	K_{Ic} (MPa$\sqrt{m}$)	K_{ILME} (MPa$\sqrt{m}$)	$(da/dt)_{ss}$ (cm/s)	
				Fixed Load	Fixed Displacement
1100-0	22.7	45.5	8	1-4	~ 0
6061-T651	282.0	31.5	9	5	0.5
7075-T651	517.0	30.5	2	9	9

The highest strength material (7075) was embrittled the most (K_{ILME} = 2 MPa$\sqrt{m}$). The medium strength alloy 6061 was embrittled the least and the lowest strength K_{ILME} fell in between. This effect was even more striking when we considered K_{ILME} as a fraction of K_{Ic}. For 7075 K_{ILME} was 6.5 percent of K_{Ic}, for 6061 it was 28.6 percent, and for 1100 it was 17.6 percent. These results indicated that strength was not the most important factor determining

the degree of embrittlement as measured with K_{ILME}. This finding was contrary to results obtained on these same alloys utilizing other measures such as percent elongation to assess the onset of embrittlement (ref 8). The results presented in Reference 8 showed that as strength increased, percent elongation in a mercury environment decreased. Percent elongation could be considered as the engineering strain necessary to initiate embrittlement in unflawed material, while K_{ILME} was the stress intensity factor necessary to propagate a pre-existing crack. Thus, yield strength was an important factor in crack initiation, but not as much as in crack propagation. There were other differences among the alloys studied other than yield strength, such as chemical composition, mechanical processing, and thermal processing. The difference in K_{ILME} values measured may indeed have been the result of one of these variables. This, we could not determine in our initial, cursory study. If other metallurgical factors did account for the data reported here, then it may not be necessary to totally sacrifice strength for increased damage tolerance in a liquid metal environment.

Another measure of the severity of embrittlement was the magnitude of the steady state crack velocity. Considered first were the fixed load $(da/dt)_{ss}$ results. As strength increased, the magnitude of steady state crack velocity also increased. If a large value of $(da/dt)_{ss}$ was indicative of more severe embrittlement than a smaller value of $(da/dt)_{ss}$, then we could state that the degree of embrittlement was increased as strength increased.

---

[8]Rostoker, M. H., McCaughey, J. M., and Markus, M., Embrittlement by Liquid Metals, Reinhold, NY, 1960.

This effect of strength was expected because of the following argument. Additions of alloying elements would not change the mechanism of crack growth. Neither would such changes necessitate that a different liquid metal-solid metal reaction occur to cause embrittlement. Therefore, once a crack propagated, the only variables which could change the magnitude of crack velocity were loading condition or strength. If a crack tip was considered as an infinite stress concentration, then the stress at the crack tip was limited to the yield strength. It was not unreasonable to assume that the higher the crack tip stress, the easier it was to cause embrittled crack growth. The higher the yield strength, the greater the $(da/dt)_{ss}$ should have been.

Changes in loading condition also caused changes in $(da/dt)_{ss}$, as were observed with the fixed displacement results reported in Table II. This discovery leads us to a discussion of transport mechanisms in the mercury embrittlement of aluminum. In fixed load testing, the constant application of the load always tended to open the crack, allowing good access of the liquid metal to the crack tip. Under fixed displacement conditions, the external load was decreased in an attempt to arrest the crack. This caused the crack to close and limited the access of the mercury to the crack tip. In addition, it was safe to assume that some plastic deformation occurred in the vicinity of the crack tip during crack propagation. When the crack moved, an envelope of plastically deformed material surrounded the newly created fracture surfaces. This "plastic wake" could tend also to close the crack, further limiting the access of embrittling species to the crack tip. The same crack closure phenomenon is known to occur readily in aluminum alloys (ref 9).

---

[9]Elber, W., in Damage Tolerance in Aircraft Structures, ASTM STP 486, ASTM, Philadelphia, PA, 1971, p. 230.

Furthermore, this scenario predicted that the lowest strength alloy would develop the largest plastic wake and thus the greatest effect of crack closure. This explained the observed results.

Fatigue Loading Results

There were two measures of the degree of embrittlement in the fatigue loading results. These were the threshold of embrittled crack growth ΔK_{th} and the maximum crack growth rate. Using ΔK_{th}, the same conclusions drawn from the static loading results were made. The 7075 alloy was embrittled the most, 6061 the least, and 1100 in between. In addition, the numerical value of ΔK_{th} agreed quite well with the K_{ILME} results for the various alloys. This suggested that regardless of loading conditions, the onset of embrittled crack growth from a pre-existing crack was the same.

The maximum crack growth rates $(da/dN)_{max}$ occurred at 5 Hz, but at different ΔK values. In 1100 $(da/dN)_{max}$ was about 3×10^{-5} m/cycle at ΔK of about 10 MPa$\sqrt{m}$. For 6061 and 7075 $(da/dN)_{max}$ were 6×10^{-4} m/cycle and 2×10^{-3} m/cycle at ΔK values of 25 MPa$\sqrt{m}$ and 10 MPa$\sqrt{m}$ respectively. This was the same trend as with the fixed load $(da/dt)_{ss}$ results; the crack growth data increased with increased strength. The effect of strength on $(da/dN)_{max}$ was much greater than the effect of strength on $(da/dt)_{ss}$. The fixed load $(da/dt)_{ss}$ for 7075 was only about twice the value for 1100, while $(da/dN)_{max}$ was about 60 times greater in 7075 than 1100. Thus, the degree of embrittlement in fatigue was much more sensitive to yield strength than was the case in static loading.

The effect of loading frequency was as expected. When frequency was decreased, the crack growth rate increased. The magnitude of the change in growth rate was not as expected. It has been shown (ref 2) that the increase in crack growth rate should be directly related to the decrease in loading frequency. For our results the crack growth rate at 5 Hz should have been six times faster than the crack growth rate at 30 Hz. In all three alloys the increase with decreasing frequency was a function of ΔK. The actual factor was about 20 in 6061 and as much as 60 in 7075.

Both the effect of strength and loading frequency suggested that the mechanics of crack growth under fatigue conditions may have been different from the mechanics of crack growth under static conditions. If the static loading crack velocity limited the fatigue crack growth rate, then $(da/dN)_{max}$ should have been on the order of one cm/cycle regardless of the alloy at 5 Hz. Therefore, the full effect of the liquid mercury was not observed in the data under fatigue conditions. The reason for this may have been the crack closure phenomenon explained above. The results indicated that more studies should be undertaken to fully understand the fatigue crack growth phenomenon.

SUMMARY AND CONCLUSION

The crack growth behavior of three aluminum alloys tested in mercury under three different loading conditions has been studied. The behavior was not unlike other forms of environmental attack (i.e., hydrogen embrittlement of steel), but some differences occurred. There was an effect of loading

---

[2]Wei, R. P. and Landes, J. D., Matls. Res. Stand., Vol. 9, No. 7, 1969, p. 9.

condition, cracks grew faster in load control tests than in displacement control tests for the two lower strength alloys. This was attributed to a closure phenomenon. In fatigue loading, cracks grew more slowly than was expected based on a superposition of the static loading conditions. The appearance of the fracture surfaces was the same regardless of loading conditions, thus the slower crack growth in fatigue was not due to a fundamental material behavior difference. Slower crack growth must have been the result of the inability of the embrittling species to access the crack tip.

REFERENCES

1. Wei, R. P., Novak, S. R., and Williams, D. P., Matls. Res. Stand., Vol. 12, 1972, p. 25.
2. Wei, R. P. and Landes, J. D., Matls. Res. Stand., Vol. 9, No. 7, 1969, p. 9.
3. Clark, W., J. of Materials for Energy Systems, Vol. 1, 1980, p. 35.
4. Gross, B. and Srawley, J. E., "Stress Intensity Factors For Boundary Collocations for Single-Edge-Notch Specimens Subject to Splitting Forces," NASA TN D-3295, 1966.
5. Kapp, J. A., "Crack Growth in Mercury Embrittled Aluminum Alloys Under Cyclic and Static Loading Conditions," Ph.D. Thesis, Rensselaer Polytechnic Institute, Troy, NY, May 1982.
6. Kapp, J. A., Newman, J. C. Jr., and Underwood, J. H., Journal of Testing and Evaluation, JTEVA, Vol. 8, No. 6, November 1980.
7. Wei, R. P., in Fatigue Mechanisms, Fong, J. T., Ed., ASTM STP 675, ASTM, Philadelphia, PA, 1979, p. 816.
8. Rostoker, M. H., McCaughey, J. M., and Markus, M., Embrittlement by Liquid Metals, Reinhold, NY, 1960.
9. Elber, W., in Damage Tolerance in Aircraft Structures, ASTM STP 486, ASTM, Philadelphia, PA, 1971, p. 230.

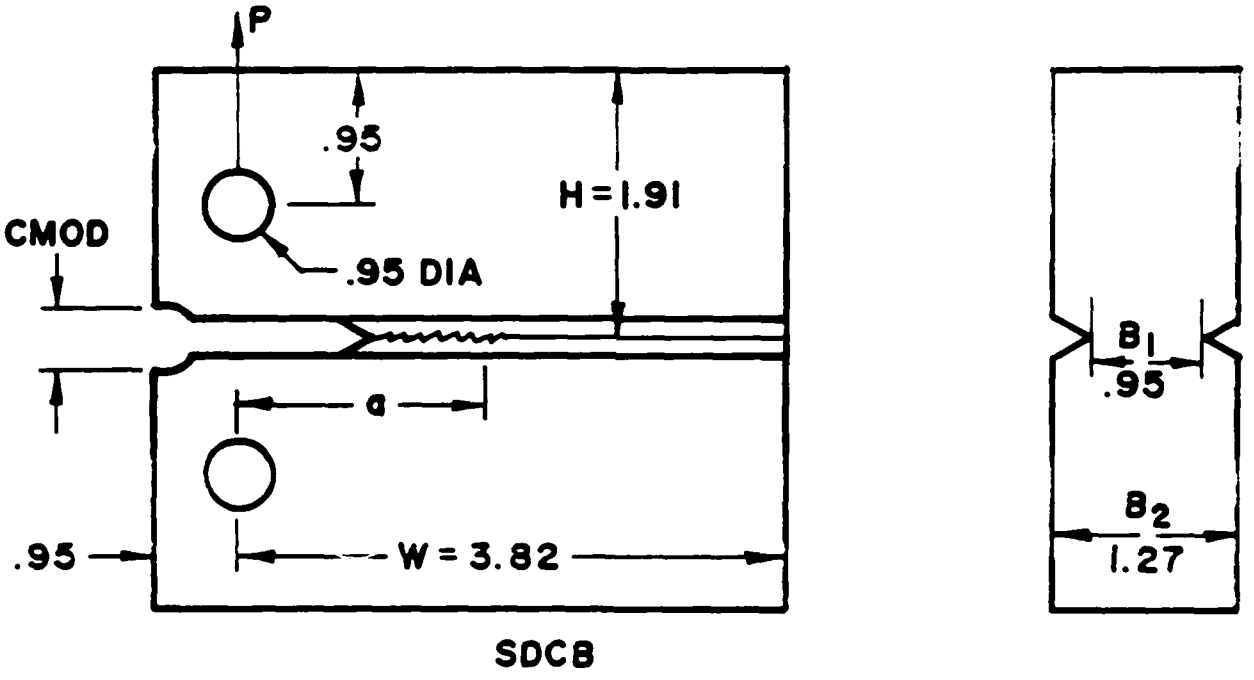

Figure 1. Crack growth specimen.

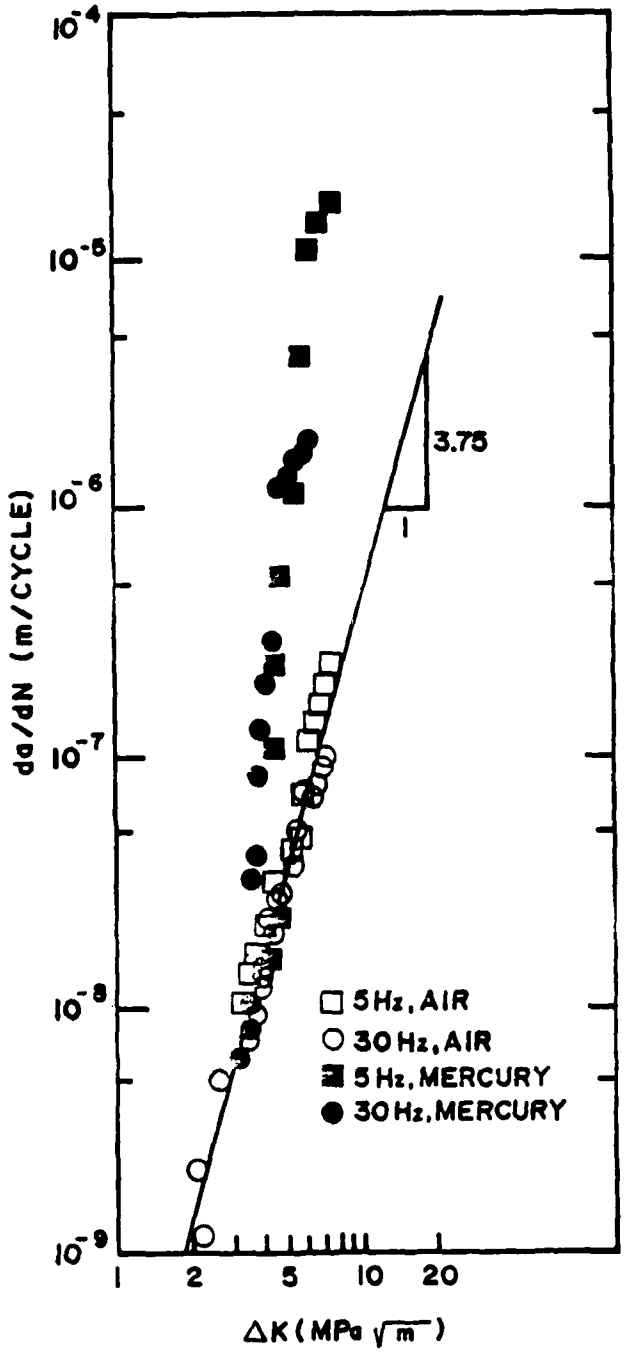

Figure 2. Fatigue loading results for 1100-0.

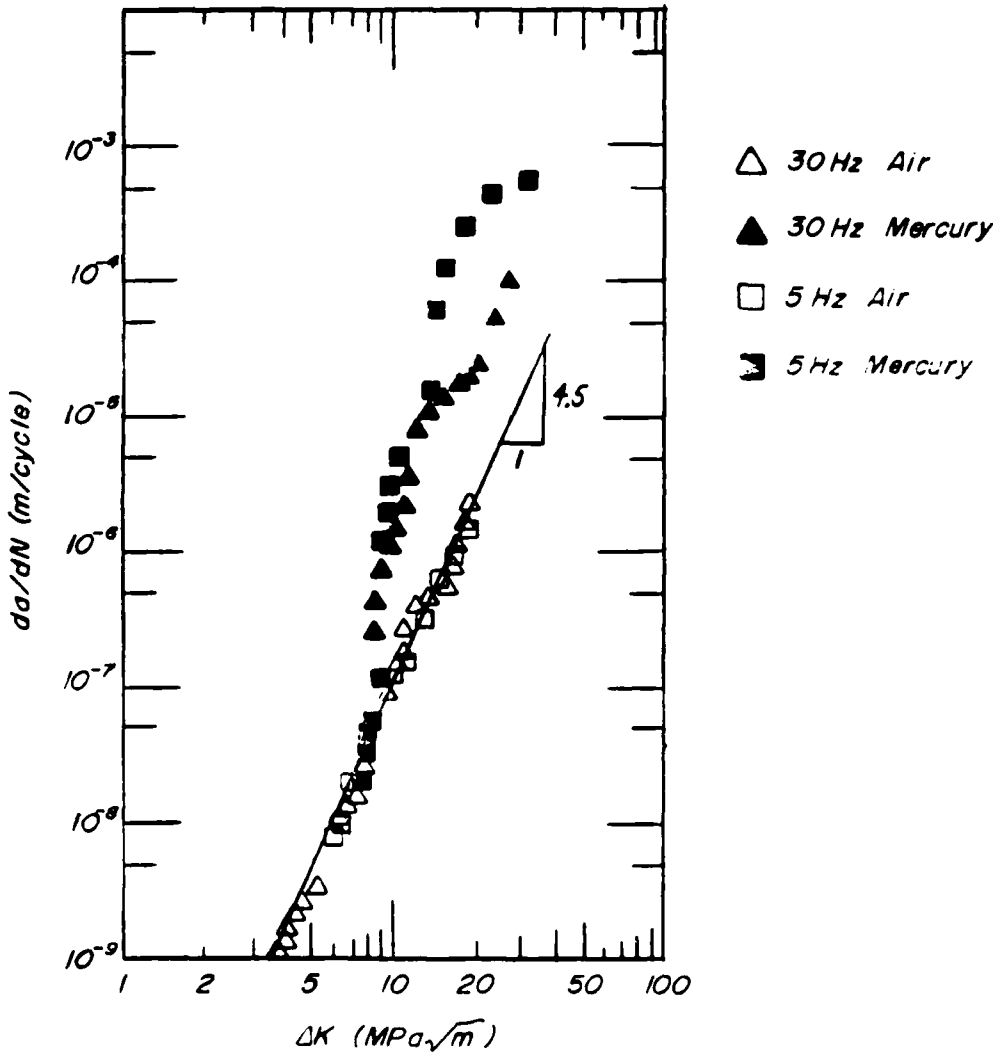

Figure 3. Fatigue loading results for 6061-T651.

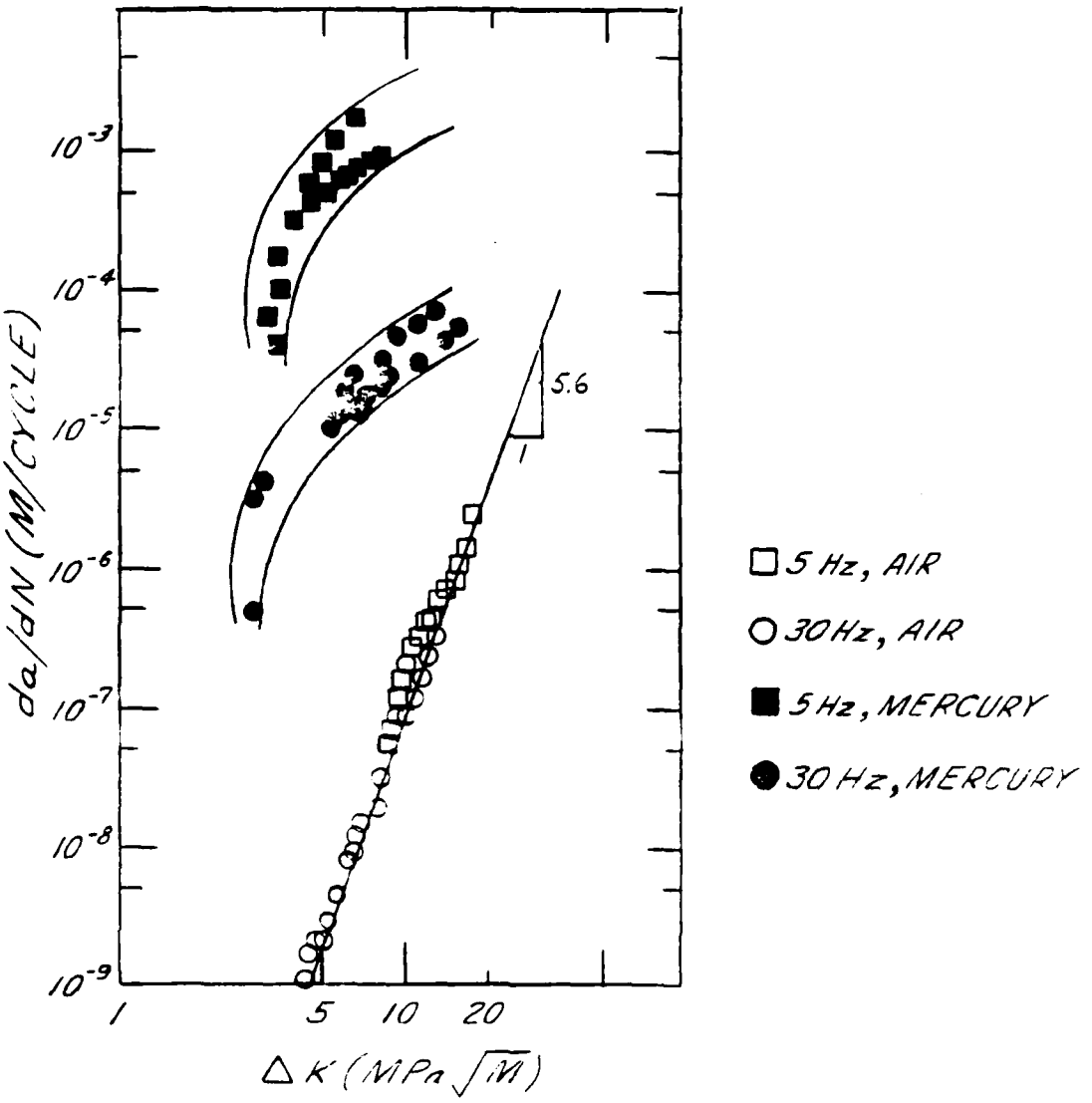

Figure 4. 7075-T651 Fatigue loading results.

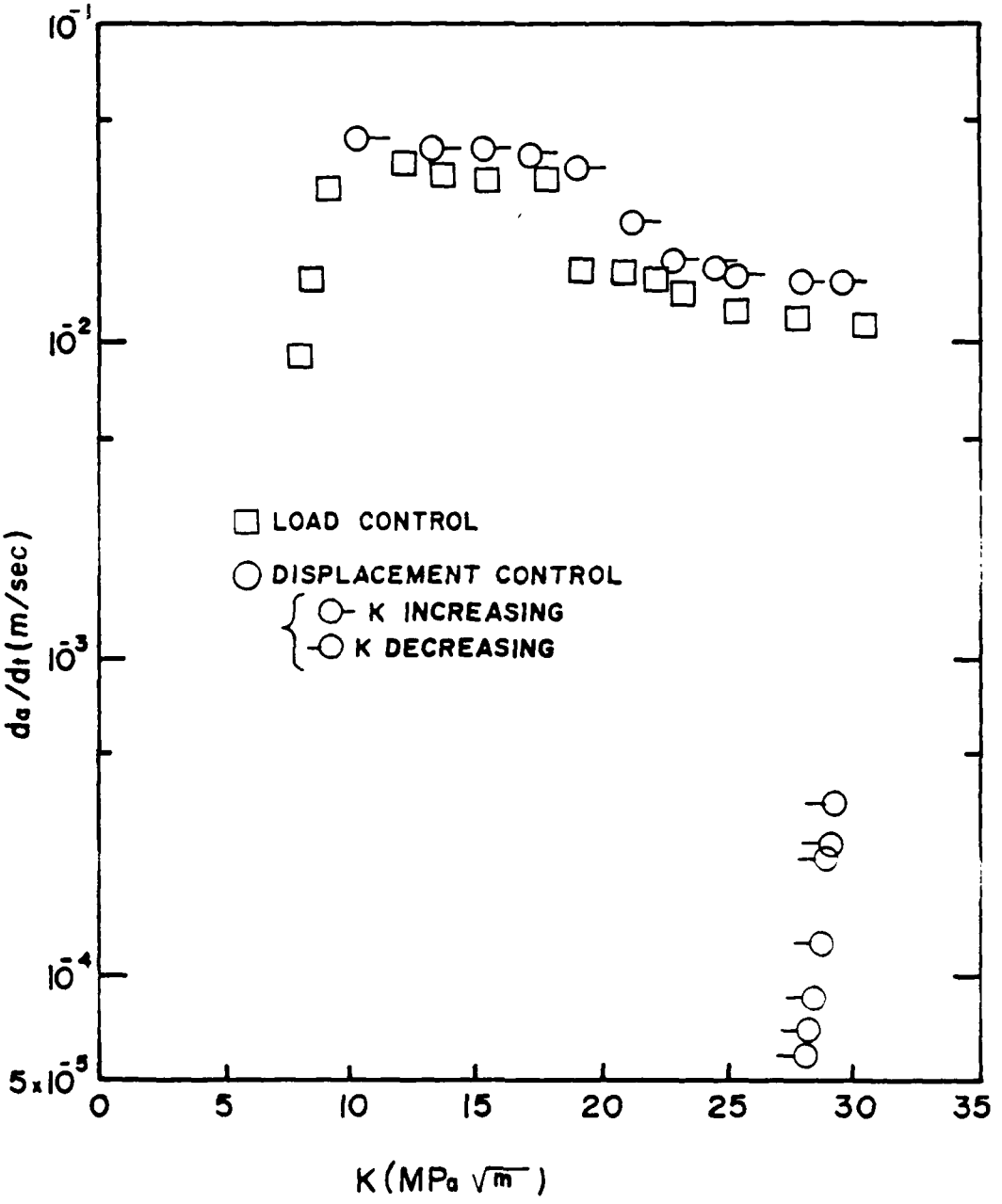

Figure 5. Static loading results for 1100-0.

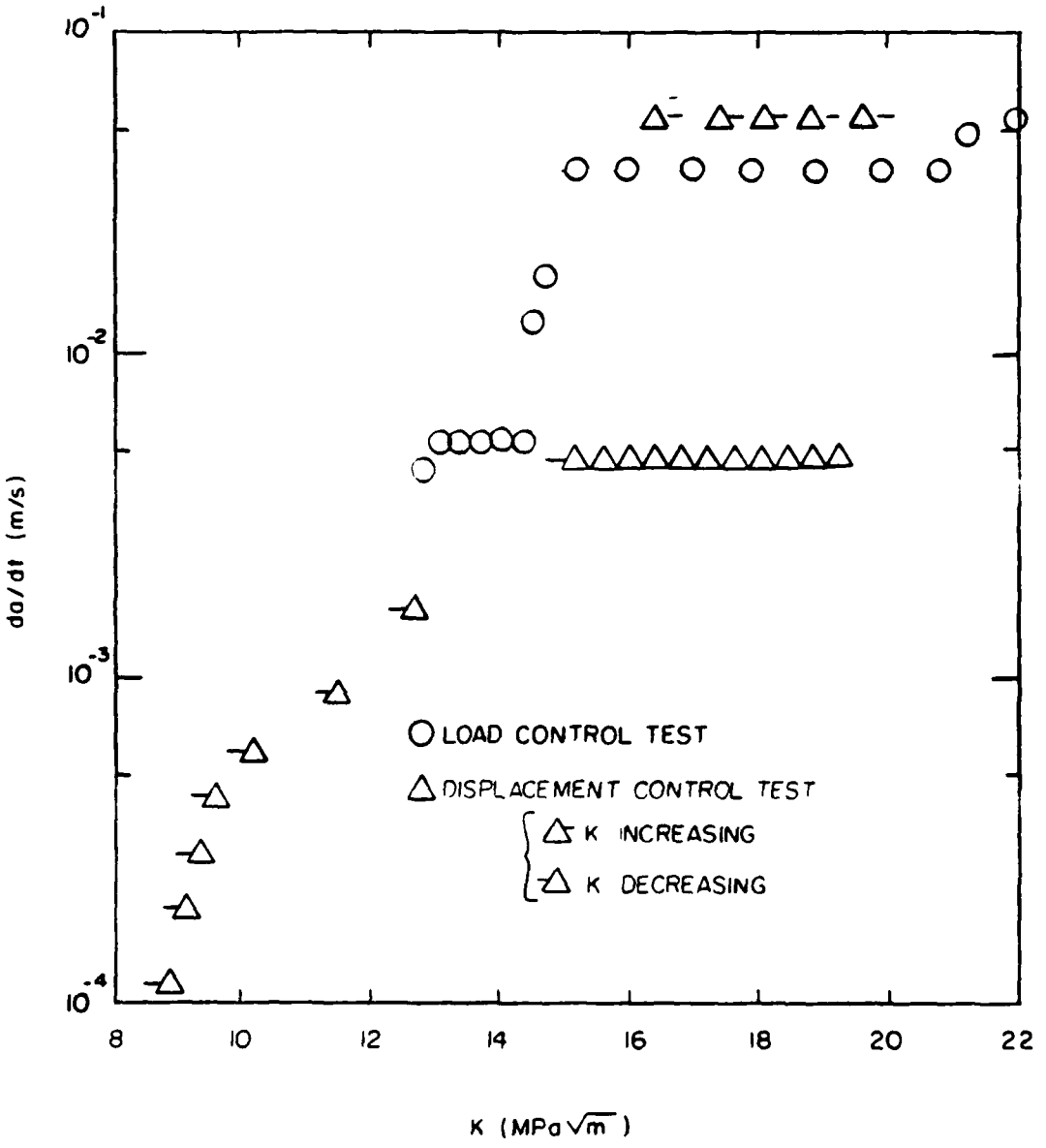

Figure 6. Static loading results for 6061-T651.

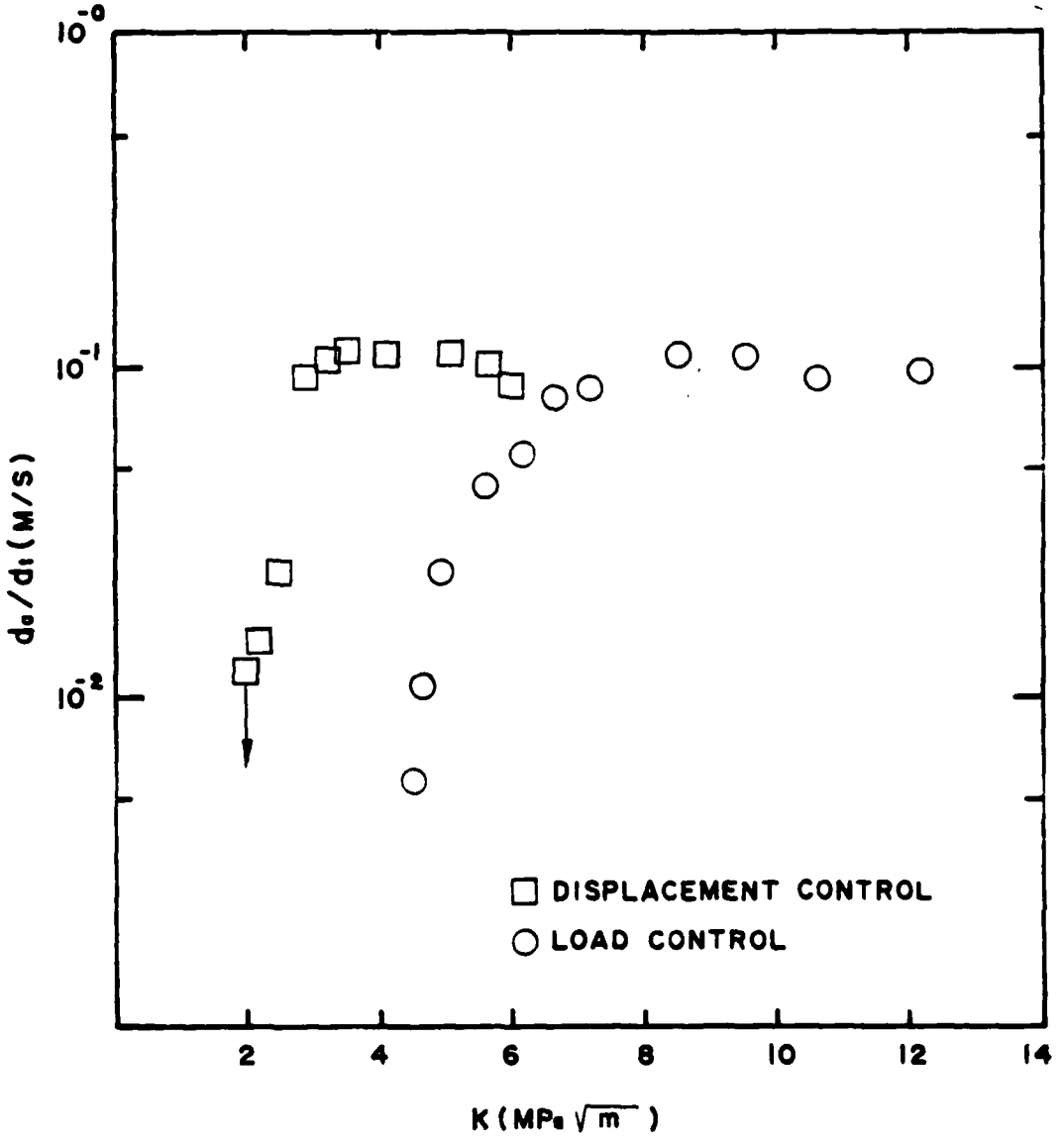

Figure 7. 7075-T651 Static loading results.

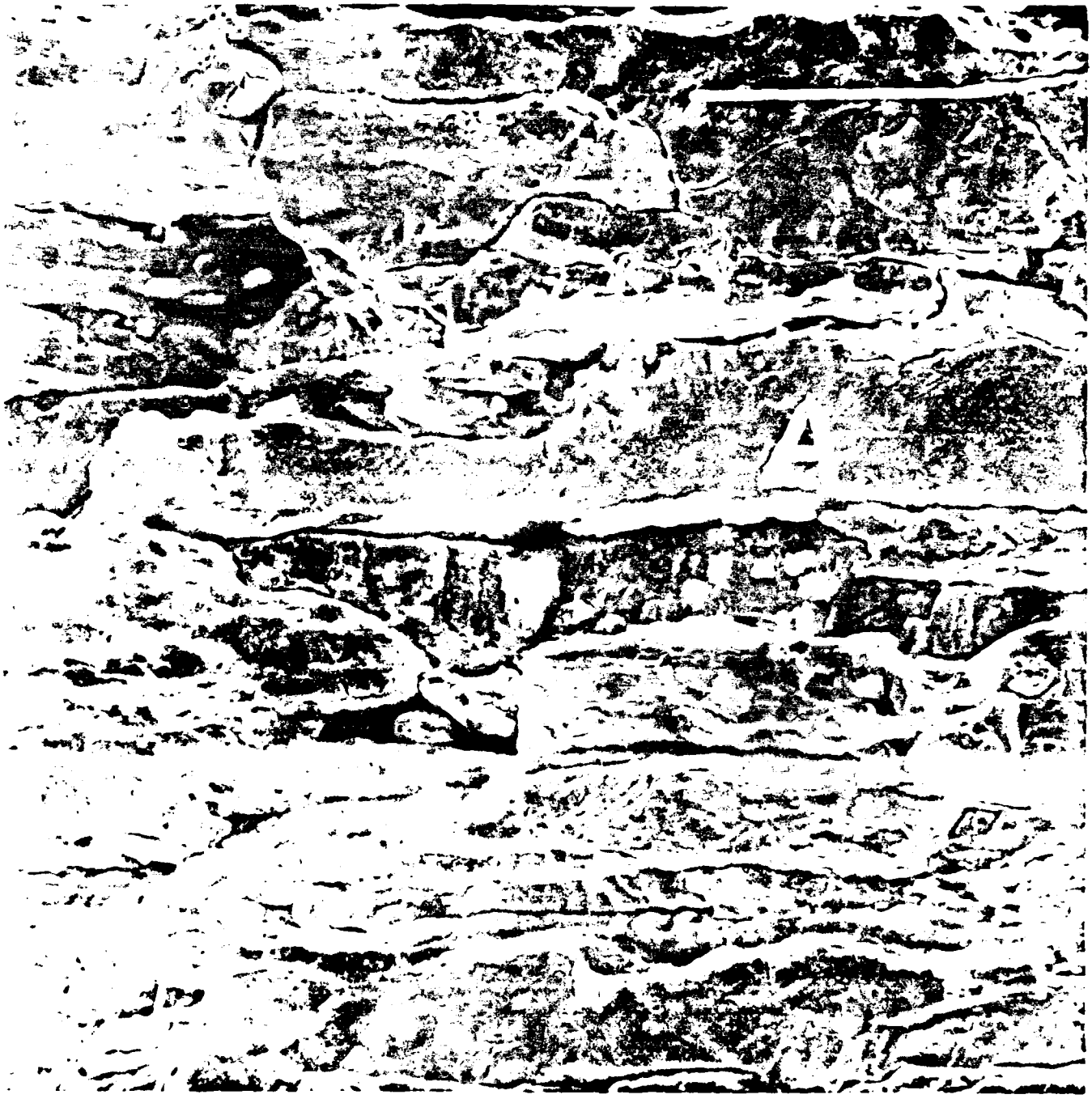

Figure 8. Fracture surface in mercury under fatigue loading conditions for 1100-0, $\Delta K > 5$ MPa$\sqrt{m}$, Crack growth in the LS plane. The marker is 100 um.

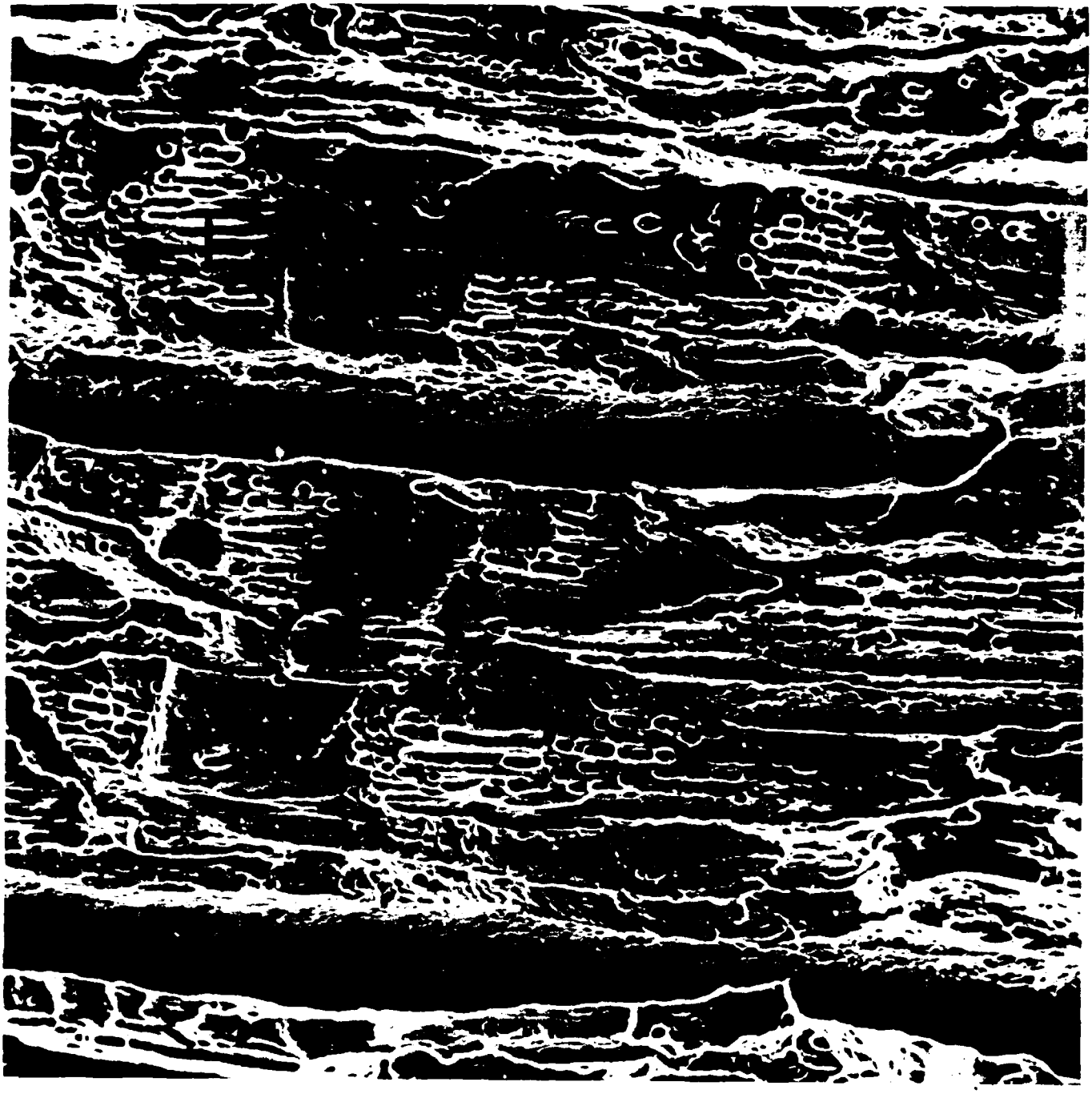

Figure 9. Fracture surface in mercury under fixed load conditions for 1100-1, $K > \sim 8$ MPa$\sqrt{m}$. The marker is 100 μm.

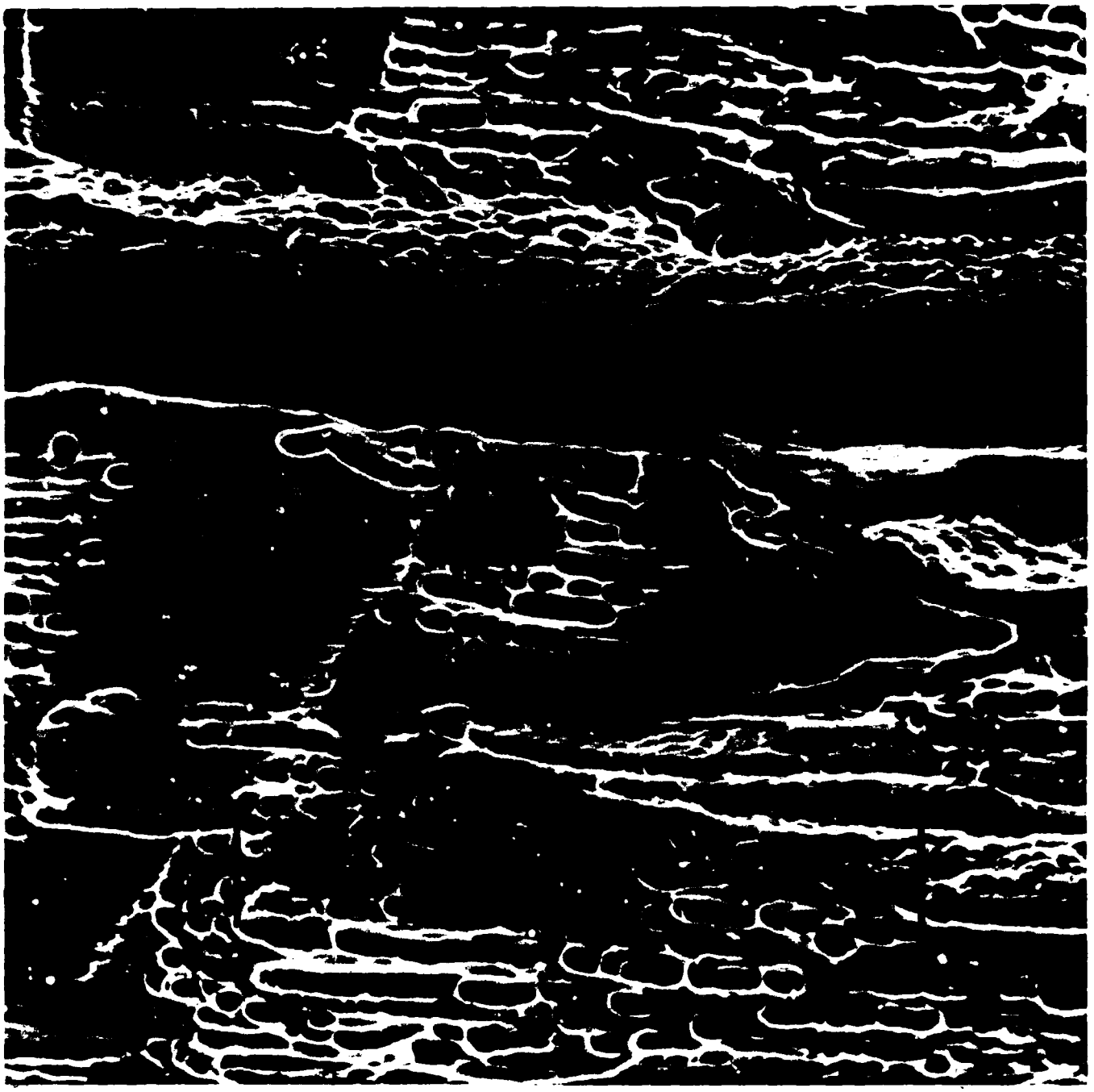

Figure 10. Higher magnification of Figure 9 showing dimples. The marker is 100 μm.

Figure 11. Fracture appearance in mercury under fixed displacement conditions for 1100-0, $K > \sim 8$ MPa$\sqrt{m}$. The marker is 100 μm.

Figure 12. Fracture appearance in mercury under fatigue loading conditions for 6061-T651, $\Delta K > \sim 8$ MPa$\sqrt{m}$, either 5 Hz or 30 Hz. The marker is 100 μm.

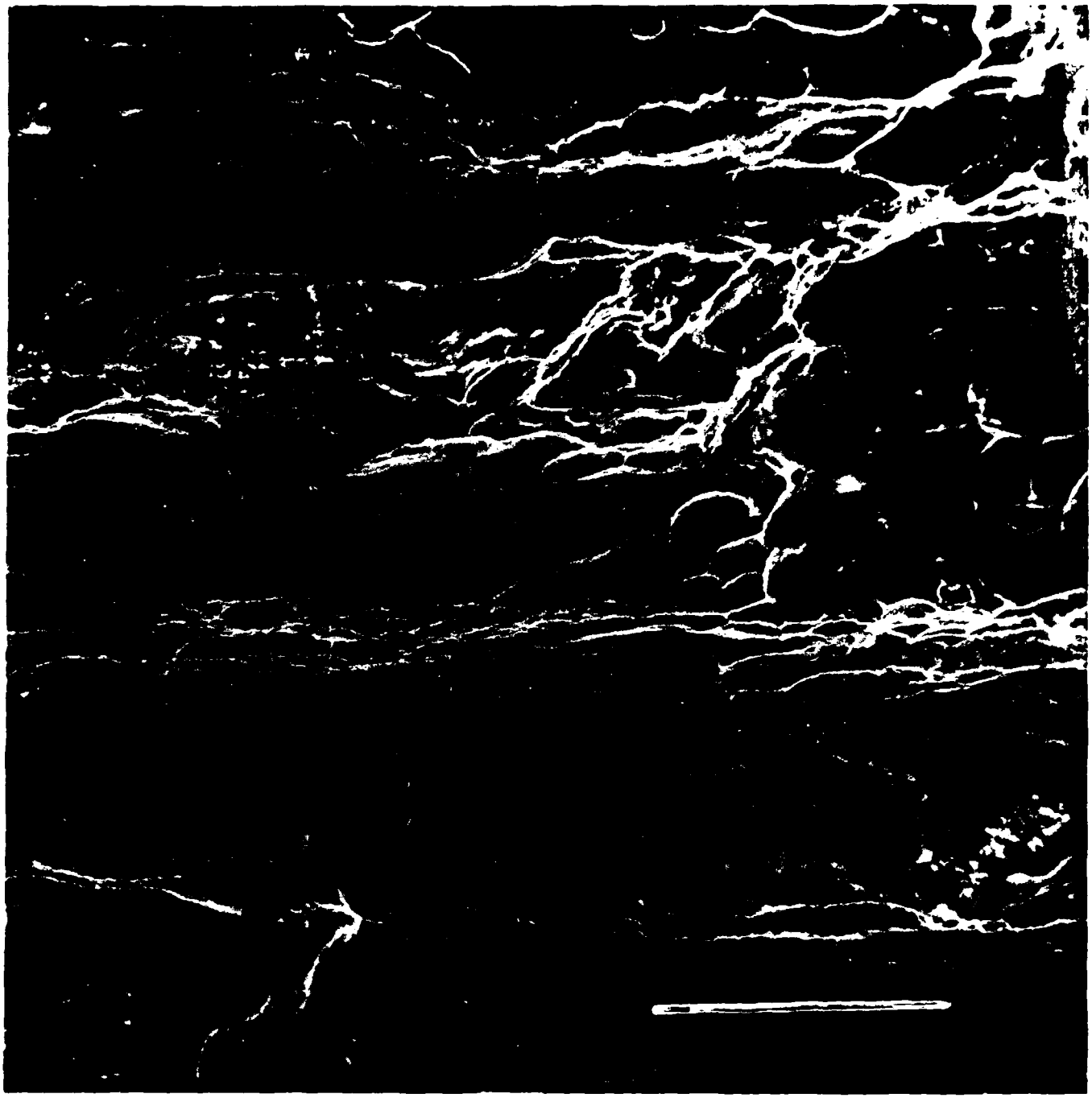

Figure 13. Fracture appearance in mercury under static loading conditions for 6061-T651, $K > \sim 9$ MPa$\sqrt{m}$. The marker is 100 μm.

Figure 14. Fracture appearance in mercury under cyclic loading conditions for 7075-T651, $\Delta K > \sim 3$ MPa$\sqrt{m}$, 5 Hz or 30 Hz. The marker is 50 μm.

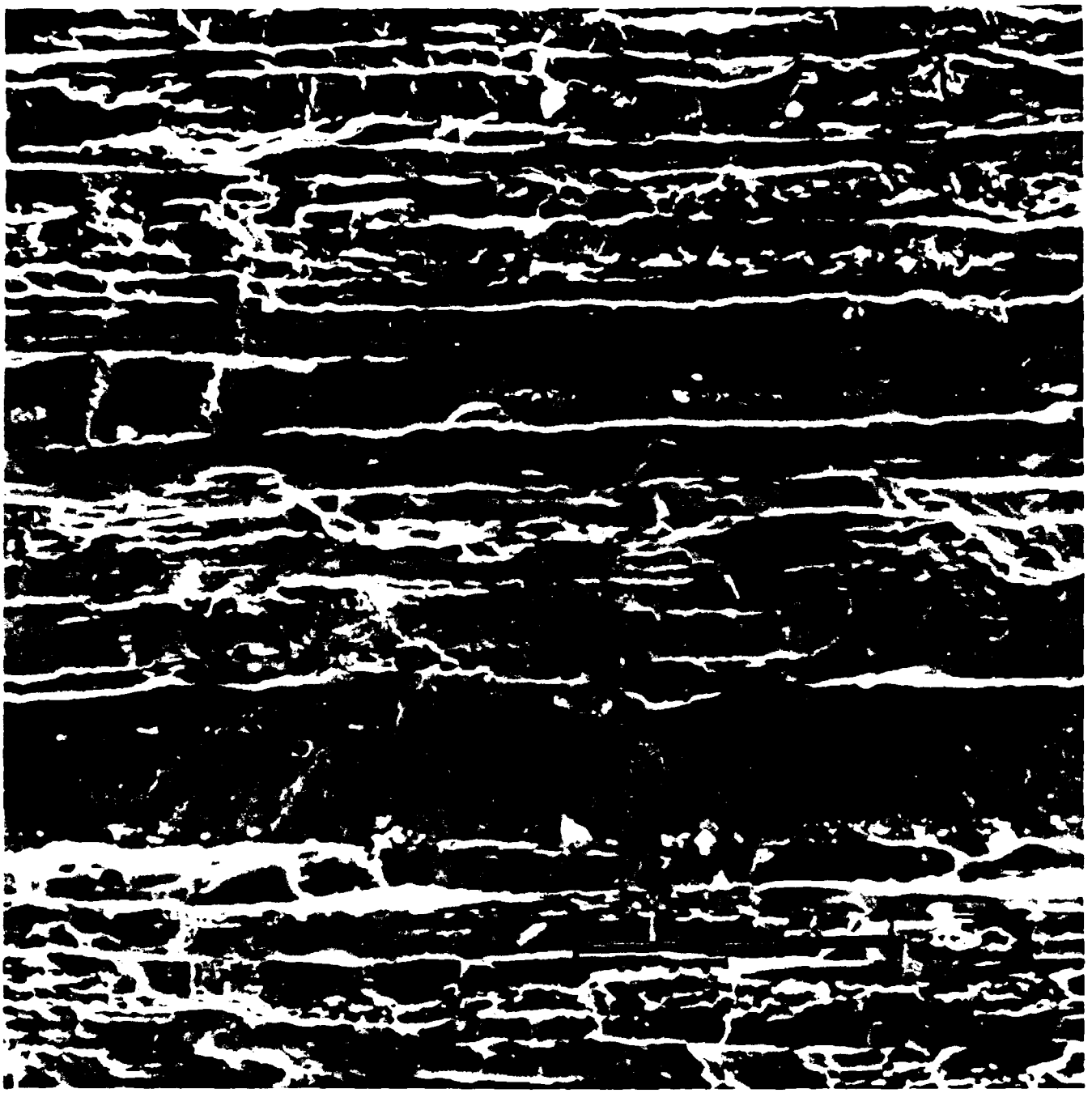

Figure 15. Fracture appearance in mercury under displacement control static loading conditions for 7075-T651, $K > \sim 2$ MPa$\sqrt{m}$. The marker is 50 μm.

TECHNICAL REPORT INTERNAL DISTRIBUTION LIST

	NO. OF COPIES
CHIEF, DEVELOPMENT ENGINEERING BRANCH	
ATTN: SMCAR-LCB-D	1
-DA	1
-DP	1
-DR	1
-DS (SYSTEMS)	1
-DS (ICAS GROUP)	1
-DC	1
-DM	1
CHIEF, ENGINEERING SUPPORT BRANCH	
ATTN: SMCAR-LCB-S	1
-SE	1
CHIEF, RESEARCH BRANCH	
ATTN: SMCAR-LCB-R	2
-R (ELLEN FOGARTY)	1
-RA	1
-RM	2
-RP	1
-RT	1
TECHNICAL LIBRARY	5
ATTN: SMCAR-LCB-TL	
TECHNICAL PUBLICATIONS & EDITING UNIT	2
ATTN: SMCAR-LCB-TL	
DIRECTOR, OPERATIONS DIRECTORATE	1
DIRECTOR, PROCUREMENT DIRECTORATE	1
DIRECTOR, PRODUCT ASSURANCE DIRECTORATE	1

NOTE: PLEASE NOTIFY DIRECTOR, BENET WEAPONS LABORATORY, ATTN: SMCAR-LCB-TL, OF ANY ADDRESS CHANGES.

TECHNICAL REPORT EXTERNAL DISTRIBUTION LIST

	NO. OF COPIES
ASST SEC OF THE ARMY RESEARCH & DEVELOPMENT ATTN: DEP FOR SCI & TECH THE PENTAGON WASHINGTON, D.C. 20315	1
COMMANDER DEFENSE TECHNICAL INFO CENTER ATTN: DTIC-DDA CAMERON STATION ALEXANDRIA, VA 22314	12
COMMANDER US ARMY MAT DEV & READ COMD ATTN: DRCDE-SG 5001 EISENHOWER AVE ALEXANDRIA, VA 22333	1
COMMANDER ARMAMENT RES & DEV CTR US ARMY AMCCOM ATTN: SMCAR-LC SMCAR-LCE SMCAR-LCM (BLDG 321) SMCAR-LCS SMCAR-LCU SMCAR-LCW SMCAR-SCM-O (PLASTICS TECH EVAL CTR, BLDG. 351N) SMCAR-TSS (STINFO) DOVER, NJ 07801	1 1 1 1 1 1 1 2
DIRECTOR BALLISTICS RESEARCH LABORATORY ATTN: AMXBR-TSB-S (STINFO) ABERDEEN PROVING GROUND, MD 21005	1
MATERIEL SYSTEMS ANALYSIS ACTV ATTN: DRXSY-MP ABERDEEN PROVING GROUND, MD 21005	1
COMMANDER US ARMY AMCCOM ATTN: SMCAR-ESP-L ROCK ISLAND, IL 61299	1
COMMANDER ROCK ISLAND ARSENAL ATTN: SMCRI-ENM (MAT SCI DIV) ROCK ISLAND, IL 61299	1
DIRECTOR US ARMY INDUSTRIAL BASE ENG ACTV ATTN: DRXIB-M ROCK ISLAND, IL 61299	1
COMMANDER US ARMY TANK-AUTMV R&D COMD ATTN: TECH LIB - DRSTA-TSL WARREN, MI 48090	1
COMMANDER US ARMY TANK-AUTMV COMD ATTN: DRSTA-RC WARREN, MI 48090	1
COMMANDER US MILITARY ACADEMY ATTN: CHMN, MECH ENGR DEPT WEST POINT, NY 10996	1
US ARMY MISSILE COMD REDSTONE SCIENTIFIC INFO CTR ATTN: DOCUMENTS SECT, BLDG. 4484 REDSTONE ARSENAL, AL 35898	2
COMMANDER US ARMY FGN SCIENCE & TECH CTR ATTN: DRXST-SD 220 7TH STREET, N.E. CHARLOTTESVILLE, VA 22901	1

NOTE: PLEASE NOTIFY COMMANDER, ARMAMENT RESEARCH AND DEVELOPMENT CENTER, US ARMY AMCCOM, ATTN: BENET WEAPONS LABORATORY, SMCAR-LCB-TL, WATERVLIET, NY 12189, OF ANY ADDRESS CHANGES.

TECHNICAL REPORT EXTERNAL DISTRIBUTION LIST (CONT'D)

	NO. OF COPIES
COMMANDER US ARMY MATERIALS & MECHANICS RESEARCH CENTER ATTN: TECH LIB - DRXMR-PL WATERTOWN, MA 01272	2
COMMANDER US ARMY RESEARCH OFFICE ATTN: CHIEF, IPO P.O. BOX 12211 RESEARCH TRIANGLE PARK, NC 27709	1
COMMANDER US ARMY HARRY DIAMOND LAB ATTN: TECH LIB 2800 POWDER MILL ROAD ADELPHIA, MD 20783	1
COMMANDER NAVAL SURFACE WEAPONS CTR ATTN: TECHNICAL LIBRARY CODE X212 DAHLGREN, VA 22448	1
DIRECTOR US NAVAL RESEARCH LAB ATTN: DIR, MECH DIV CODE 26-27, (DOC LIB) WASHINGTON, D.C. 20375	1 1
COMMANDER AIR FORCE ARMAMENT LABORATORY ATTN: AFATL/DLJ AFATL/DLJG EGLIN AFB, FL 32542	1 1
METALS & CERAMICS INFO CTR BATTELLE COLUMBUS LAB 505 KING AVENUE COLUMBUS, OH 43201	1

NOTE: PLEASE NOTIFY COMMANDER, ARMAMENT RESEARCH AND DEVELOPMENT CENTER, US ARMY AMCCOM, ATTN: BENET WEAPONS LABORATORY, SMCAR-LCB-TL, WATERVLIET, NY 12189, OF ANY ADDRESS CHANGES.

END

FILMED

2-86

DTIC